SCIENTIFIC REPORTS

OPEN

SUBJECT AREAS:
HEALTH OCCUPATIONS
ORTHOPAEDICS

Received
4 February 2014

Accepted
27 June 2014

Published
17 July 2014

Correspondence and requests for materials should be addressed to L.S. (laura.santambrogio@einstein.yu.edu)

Molecular analysis of chromium and cobalt-related toxicity

Brian Scharf[1], Cristina C. Clement[1], Valerio Zolla[1], Giorgio Perino[2], Bo Yan[3], S. Gokhan Elci[3], E. Purdue[2], S. Goldring[2], Frank Macaluso[4], Neil Cobelli[5], Richard W. Vachet[3] & Laura Santambrogio[1,5,6]

[1]Department of Pathology, Albert Einstein College of Medicine, 1300 Morris Park Avenue, Bronx, NY, 10461, [2]Hospital for Special Surgery, 535 East 70th Street, New York, NY 10021, [3]Department of Chemistry, University of Massachusetts, Amherst, MA 01003, [4]Anatomy and Structural Biology, Albert Einstein College of Medicine, 1300 Morris Park Avenue, Bronx, NY, 10461, [5]Orthopaedic Surgery, Albert Einstein College of Medicine, 1300 Morris Park Avenue, Bronx, NY, 10461, [6]Microbiology and Immunology, Albert Einstein College of Medicine, 1300 Morris Park Avenue, Bronx, NY, 10461.

Occupational and environmental exposure to Co and Cr has been previously linked to a wide array of inflammatory and degenerative conditions and cancer. Recently, significant health concerns have been raised by the high levels of Cr and Co ions and corrosion products released by biomedical implants. Herein, we set to analyze the biological responses associated with Co and Cr toxicity. Histological, ultrastructural, and elemental analysis, performed on Cr and Co exposed patients reveal the presence of corrosion products, metallic wear debris and metal ions at varying concentrations. Metallic ions and corrosion products were also generated *in vitro* following macrophage phagocytosis of metal alloys. *Ex vivo* redox proteomic mapped several oxidatively damaged proteins by Cr(III) and Co(II)-induced Fenton reaction. Importantly, a positive correlation between the tissue amounts of Cr(III) and Co(II) ions and tissue oxidative damage was observed. Immobilized- Cr(III) and Co(II) affinity chromatography indicated that metal ions can also directly bind to several metallo and non-metalloproteins and, as demonstrated for aldolase and catalase, induce loss of their biological function. Altogether, our analysis reveals several biological mechanisms leading to tissue damage, necrosis, and inflammation in patients with Cr and Co-associated adverse local tissue reactions.

Living organisms require a small amount of different metals for their metabolic functions. Among them Cr and Co are important microelements which are found in trace quantities in the human body where they regulate important biological functions. Cr is involved in glucose metabolism, either by facilitating insulin binding to its receptor or by amplifying the effect of insulin on carbohydrate and lipid catabolism[1,2]. On the other hand Co(III) ions occupy the catalytic site of vitamin B12 and are essential to the vitamin's biological activity[3]. Under physiological conditions both metals need to be present only in trace quantities because they are required for the biological activity of a very small number of specific cellular proteins[4].

Cr and Co toxicity is associated with their oxidation state[4,5]. Cr can be present as a wide range of possible oxidation states (Cr(I), Cr(III), Cr(IV), Cr(V), Cr(VI)) even though Cr(III) and Cr(VI) are the most energetically stable and thus the most commonly observed[6,7]. The effects of hexavalent Cr (Cr(VI)) have been previously analyzed since it is classified as group 1 carcinogen (carcinogenic to humans) by the International Agency for Research on Cancer (IARC) mostly related to evidence of excess of malignant lung tumors in exposed workers and is also an environmental pollutant[8]. On the other hand, the mechanisms related to the toxicity of Cr(III) are still unknown[5,6] and therefore it is classified as group 3 carcinogen (unclassifiable due to lack of adequate evidence) by the IARC. Likewise Co can be found in different oxidation states among which Co(II) and Co(III) are the most common[9,10] and it is classified with its compounds as group 2B carcinogen (possibly carcinogenic to humans) by the IARC. Occupational exposure to Co has been shown to be associated with cardiomyopathy and neurological damage[11–13].

Lately, major health concerns have been raised by the toxic levels of Cr and Co released by metal-on-metal (MoM) bearing surface and also metallic junctions of hip implants used worldwide in orthopedic surgery[14,15]. Whereas in an industrial setting, the toxicity of Cr and Co is contingent upon the duration of exposure, nanoparticle concentration, and entry routes into the body across a barrier membrane (dermal or inhalation absorption), the release of Co and Cr nanoparticles from metallic orthopedic implant devices represents an internal exposure to metals that is not dependent on absorption through barrier membranes and exemplifies a still relatively unexplored field of toxicology[8]. It has been determined that these implants release particulate metal

debris in the form of corrosion with or without abrasion particles, which are non ionized metal alloys[15,16]. These non-ionized metal alloys are primarily nanometer-sized particles[8,17].

Data from the literature indicate a range of 5–100 μg/L of Cr and 5–300 μg/L of Co present in plasma and tissues from patients with MoM implants at revision surgery[18]. With regards to metal ions, it is still controversial whether Cr is present as Cr(VI) in patients with MoM bearing surface and/or metal connections, with some reports supporting this idea and others disproving it[19–21]. There is a general consensus, however, that Cr(III) is elevated in the biological fluids of all patients with MoM-type implants[22,23] and also that elevated Co(II), albeit at different levels, is found in serum, blood, and urine of all examined patients[24–26]. Histologically, an exuberant inflammatory reaction often associated with tissue necrosis/infarction, macrophagic and lymphocytic infiltrate is observed and originally defined as aseptic lymphocytic vasculitis associated lesions (ALVAL) and later revised as adverse local tissue reaction (ALTR) or adverse reaction to metallic debris (ARMD)[27,28]. This reaction is likely due to a combination of metal ion toxicity combined with a hypersensitivity reaction which is particularly enhanced in some patients for reasons still not well understood.

These types of implant release particulate metal debris in the form of corrosion particles with or without addition of abrasion particles[29]. Since it is well established that the major health risk and toxicity of Cr and Co are not related to their elemental composition (Cr^0 and Co^0) but to their oxidation state it is of fundamental importance to understand the mechanism underlying metal oxidation in biological samples[30–32]. An in depth analysis of the relationship between the concentration of Cr and Co ions[30–32] in the biological fluids and the biochemical, molecular and mechanistic analysis leading to biological damage is still missing. The surgical implantation of orthopedic implants represents a "controlled" model for examining the toxicity and mechanism of action of Co and Cr since there are well-defined parameters including duration of exposure and chemical composition of the implant. In this study, peri-implant tissues from revision surgeries were employed to examine the interaction between Cr and Co ions with tissue biomolecules and their relationship with the adverse tissue reaction.

Results

Histological analysis of metal wear debris in periprosthetic tissues MoM implants. Histological examination of periprosthetic tissues recovered from patients with MoM implants demonstrated in some cases the occurrence of the classic layering of a high grade advanced adverse reaction with a thick superficial layer of necrosis/infarction, intermediate layer of macrophagic and lymphocytic infiltrate, and deep layer of perivascular lymphoplasmacytic infiltrate (Figure 1a) associated with presence of large aggregates of corrosion particles of variable size in at least one histological section in most of the examined revision tissues (Figure 1b). Globular and/or irregular small particles of corrosion products were also observed in exfoliated (Figure 1c) and interstitial macrophages (Figure 1d). Ultrastructural analysis of the same case revealed phagosomes filled with predominantly round electron dense particles of variable intensity consistent with corrosion products and a few rod-shaped particles consistent with metallic abrasion particles not identifiable at light microscopy (Figure 1e). Particulate debris was present in the cytoplasm of the macrophages and interstitially as both electron dense rod-shaped and irregular particles and less electron dense, spherical particles that ranged from nanometer to micrometer in size (Figure 1e, 1f, 1g).

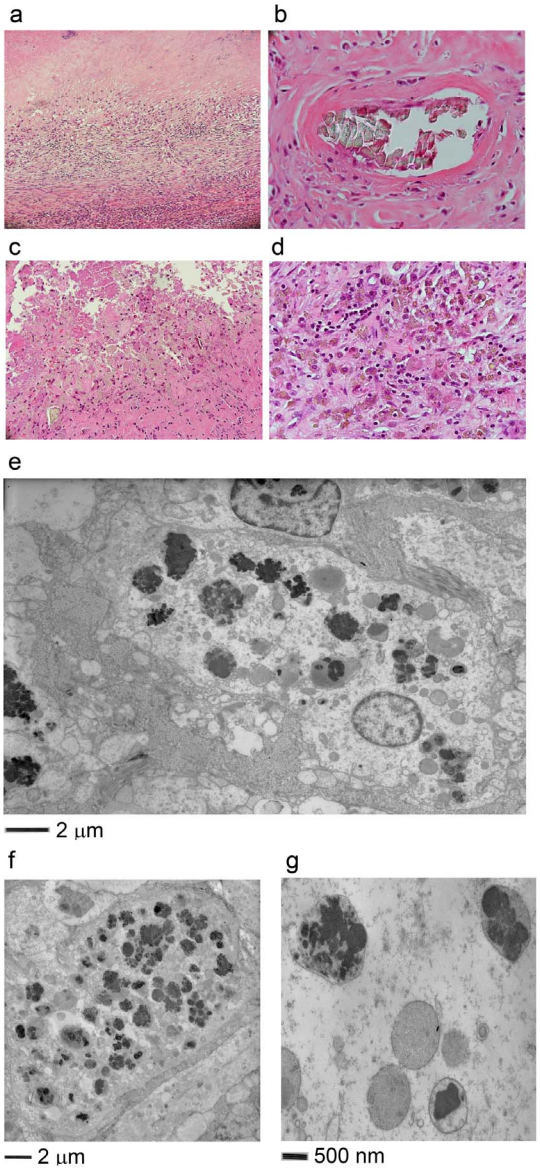

Figure 1 | Corrosion products and metal wear debris in periprosthetic tissues. (a) Necrosis and macrophagic-lymphocytic infiltrate in the periprosthetic soft tissue of a MoM implant with metallic sleeve adapter (H-E stain). (b) Large aggregate of pale green-reddish corrosion particles with sheet-like crystalline structure in the periprosthetic soft tissue (H-E stain). (c) Macrophagic exfoliation with release of corrosion products. (d) Macrophagic infiltrate containing pale green globular particles of similar material (H-E stain). (e) Ultrastructural analysis of nanometer and micrometer size particles of a macrophage from the same area as shown in (b). (f) Ultrastructural analysis of partially phagocytosed particulate debris within the endosomal compartments of a macrophage. (g) Higher magnification showing globular particles of material with variable electron density consistent with corrosion products and an irregular particle of high electron dense most probably representing abrasion induced metallic debris.

Increased cobalt and chromium accumulation in periprosthetic tissues surrounding MoM implants. Periprosthetic tissues were collected from 18 patients undergoing hip revision surgery (Table 1). Metal ion concentrations were measured in periprosthetic tissues surrounding MoM implants (9 cases) and in revision tissues from alternative bearings revision samples (9 cases), including metal-on-polyethylene (MoP), ceramic-on-polyethylene (CoP), and ceramic-on-ceramic (CoC).

A significant increase in Co and Cr accumulation was detected in revision samples surrounding MoM implants as compared to control (alternative bearings) tissues (Figures 2a, 2b). Inductively coupled plasma mass spectrometry (ICP-MS) measurements revealed a 2.5-

Table 1 | Patient demographics and information regarding prostheses

Patient #	Age	Sex	Implant type	Duration of implant	Reason for revision
1	73	F	MoP	57 months	Dislocation
2	54	F	MoP	37 months	Dislocation
3	76	M	MoP	81 months	Osteolysis
4	69	F	MoP	101 months	Osteolysis
5	79	M	MoP	78 months	Osteolysis
6	81	F	CoP	124 months	Osteolysis
7	43	F	CoP	24 months	Dislocation
8	49	M	CoP	38 months	Mechanical Failure
9	69	M	CoC	80 months	Dislocation
10	45	F	MoM Resurfacing	19 months	ALTR
11	52	F	MoM Resurfacing	63 months	ALTR
12	44	F	MoM Resurfacing	34 months	ALTR
13	43	M	MoM Resurfacing	72 months	ALTR
14	47	M	MoM THA	52 months	ALTR
15	71	M	MoM THA	58 months	ALTR
16	56	F	MoM THA	36 months	ALTR
17	67	M	MoM THA	21 months	ALTR
18	64	F	MoM THA	61 months	ALTR

MoP: metal on polyethylene; CoP: ceramic on polyethylene; CoC: ceramic on ceramic; MoM: metal on metal.
THA: total hip arthroplasty; ALTR: adverse local tissue reaction.
Note: All patients did not have occupational exposure or known leisure exposure to products containing significant amounts of cobalt or chromium.

fold increase of tissue Co levels surrounding MoM implants as compared to controls (Figure 2a). Periprosthetic tissue Cr levels from MoM implants were found to be 9-fold higher as compared to controls (Figure 2b).

To determine the elemental composition of wear particles, backscatter SEM coupled with energy-dispersive X-ray spectroscopy (EDS) was used to examine wear debris powders accumulated in metallic sleeve adapters. EDS spectra demonstrate that both Cr and Co were present in implant wear debris (Figure 2c).

Metal ions are produced from phagocytosed Co or Cr nanoparticles in macrophage endosomal compartments. The confirmation of elevated Co and Cr levels in the periprosthetic tissues surrounding MoM implants led to the next series of experiments aimed at addressing the mechanism(s) underlying the formation of metal ions. Histological analysis of the tissues surrounding the tested implants revealed extensive macrophagic infiltrates with phagocytosed pale green corrosion products and in the pictured case, abrasion black metallic particles secondary to implant impingement were also present (Figure 3a). Ultrastructural examination of MoM revision tissue demonstrated that nanometer size electron dense wear debris particles are phagocytosed by macrophages in the periprosthetic tissue (Figure 3b). An accumulation and engorgement of late endosomes and lysosomes, with needle-shaped and spherical wear debris particles, were observed in macrophages present in revision tissues (Figure 3c).

The accumulation of phagocytosed wear debris in late endosomal and lysosomal compartments prompted us to examine the effects of the acidic, highly proteolytic micro-environment of these organelles on metal nanoparticles. Wild-type C57Bl/6 bone marrow macrophages were left untreated or exposed to cobalt or chromium nanoparticles at concentrations of 10^9, 10^{10}, 10^{11}, and 10^{12} particles per ml for 12 hours. Macrophages treated with cobalt or chromium nanoparticles demonstrated a dose- dependent increase in cobalt and chromium ions concentrations, as measured spectrophotometrically (Figures 3d, 3e). The observed increase in cobalt and chromium ion levels led us to examine the relationship between pH and metal ion generation. To this end we incubated primary macrophages in the presence or absence of NH_4Cl and leupeptin, prior to treatment with chromium nanoparticles. The pre-treatment of cells with a combination of NH_4Cl and leupeptin makes the intralysosomal pH more basic and inhibits lysosomal proteolysis, respectively. Macrophage chromium ion levels were determined 12 hours following nanoparticle exposure. Chromium ion levels were significantly elevated in macrophages exposed to nanoparticles alone as compared to cells pre-treated with lysosomal inhibitors and control cells. With increasing concentrations of nanoparticle exposure, NH_4Cl and leupeptin pre-treated cells did not demonstrate a significant elevation of chromium ion release. Cells not pre-treated with NH_4Cl and leupeptin, however, revealed a dose dependent increase in chromium ion levels following nanoparticle exposure (Figure 3f).

Chromium orthophosphate ($CrPO_4$) is among the most commonly observed implant corrosion products in the periprosthetic tissue and it is due to the precipitation of chromium and phosphate ions. The observation of phagocytosed $CrPO_4$ within macrophagic dominant infiltrates prompted us to examine the effects of endosomal/lysosomal microenvironment on $CrPO_4$, and particularly whether Cr ions could be released from $CrPO_4$. Primary macrophages were left untreated or exposed to increasing concentrations of $CrPO_4$ (Figure 3g). A dose-dependent increase in chromium ion release was measured in cells exposed to $CrPO_4$ (Figure 3h).

Histological examination of infiltrates with phagocytosed corrosion products demonstrated a transition from healthy to degenerated macrophages with foamy elements in the periprosthetic tissues surrounding MoM implants (Figure 3i). Together, these data indicate that phagocytosed corrosion products and also abraded metallic wear debris accumulate within late endosomes with the resultant release of metal ions.

Metal ion exposure increases oxidative stress and protein carbonylation. In the next series of experiments, we examined the relationship between metal ion formation and cellular free radical production. Primary macrophages were left untreated or exposed to cobalt or chromium ions at concentrations of 10, 100, and 1000 μM for 12 hours. Using a DiOxyQ probe that fluoresces upon reacting with free radicals, significant increases in ROS levels were measured in primary macrophages exposed to cobalt or chromium at concentrations of 100 μM and 1000 μM when compared to controls (Figure 4a). Significant increases in ROS production were detected in culture supernatants from chromium or cobalt exposed cells at all concentrations when compared to controls (Figure 4b).

Next, we investigated whether elevated concentrations of cellular ROS would result in an increase of oxidatively modified proteins in macrophages exposed to metal ions. To address this aim, the cytosol

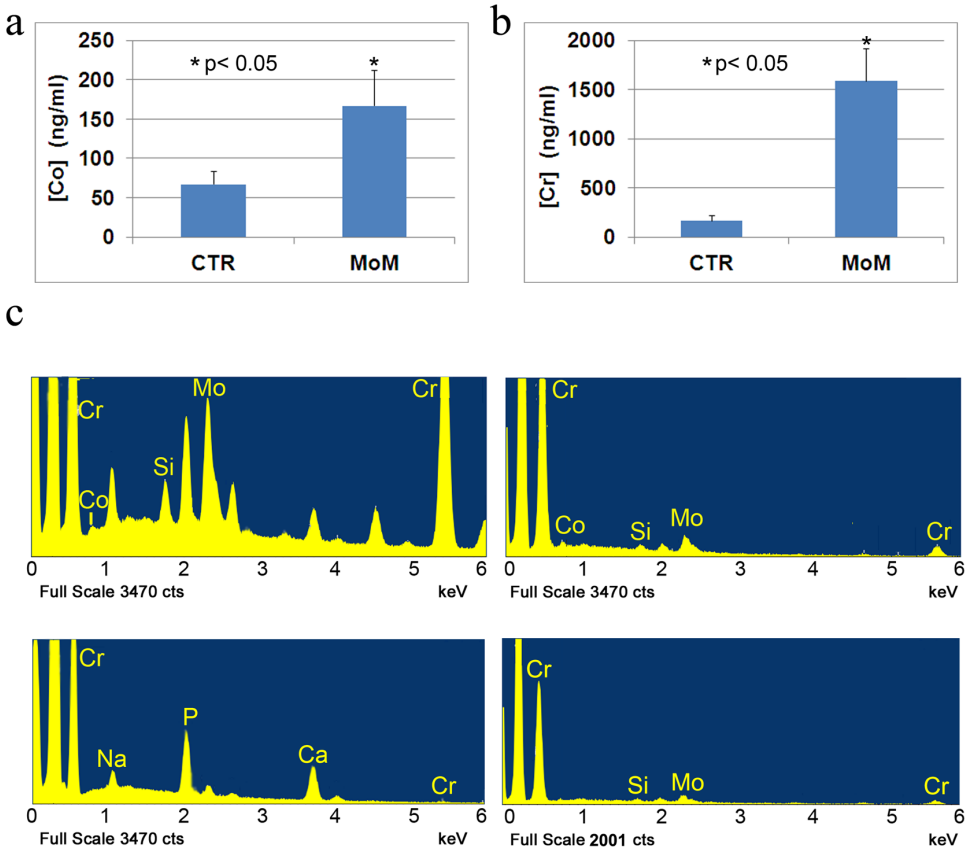

Figure 2 | Bioaccumulation of Cobalt (Co) and Chromium (Cr) in periprosthetic tissues. (a) Co ion concentrations in periprosthetic tissues surrounding control (CTR) and metal-on-metal (MoM) implants, as detected by inductively coupled plasma mass spectrometry (ICP-MS). Significant differences in Co concentrations among groups were determined using one way ANOVA ($p < 0.05$). (b) Cr ion concentrations in periprosthetic tissues surrounding control (CTR) and metal-on-metal (MoM) implants, as detected by inductively coupled plasma mass spectrometry (ICP-MS). Significant differences in Cr concentrations among groups were determined using one way ANOVA ($p < 0.05$). (c) Backscatter scanning electron microscopy and Energy-dispersive X-ray spectroscopic (EDS) analysis of wear debris retrieved from metallic sleeves. Analysis of the EDS spectra demonstrated the presence of Cr, Co, and Mo in implant wear debris.

and mitochondria were isolated from untreated and metal ions exposed cells, and subsequently incubated with 2,4-dinitrophenylhydrazine (DNPH). DNPH selectively reacts with or derivatizes carbonyl groups. The DNPH-derivatized samples were separated by a 4–15% gradient SDS PAGE, followed by western blot analysis employing an anti- DNPH primary antibody. Western blot analysis detected carbonylated proteins in the cytosol and mitochondria from untreated and cobalt or chromium exposed macrophages (Figure 4c) A significant increase in the levels of oxidatively modified proteins was detected in the cytosol and mitochondria isolated from cobalt or chromium treated cells when compared to controls (Figure 4c). Western blot analysis of primary macrophages exposed to $CrPO_4$ demonstrated a dose dependent increase in the levels of protein carbonylation in $CrPO_4$ exposed cells as compared to untreated cells. (Figure 4d).

Following the observed increases in cellular ROS levels and protein carbonylation in primary macrophages exposed to metal ions and $CrPO_4$, in addition to the significant elevation of metal ions measured in periprosthetic tissues surrounding MoM implants, the next experiments were designed to examine revision tissues surrounding hip implants for protein oxidation. The carbonyl content (carbonylated Arg, Lys, His, and Pro residues) in revision tissues was analyzed spectrophotometrically at an absorbance of 375 nm following the reaction of carbonylated amino acid side-chains of oxidized proteins with DNPH. A significant increase in carbonyl content was detected in revision tissues surrounding MoM implants as compared to control tissues (Figure 4e).

The introduction of carbonyl groups into amino acid side chains can result in the loss of catalytic or structural function of the affected protein. Thus, total proteomic analyses were performed on the proteins extracted from revision tissues surrounding MoM implants to identify peptides and proteins with posttranslational modifications, including oxidation sites. The extracted total proteome from MoM tissue homogenates was fractionated on a FPLC gel filtration column subjected to protease digestion with endoproteinase Lys-C and trypsin, and analyzed by tandem mass spectrometry (MS/MS) on a nano LC/Orbitrap system. Nano LC-ESI-MS/MS analysis demonstrated substantial oxidation of amino acids of several proteins in the periprosthetic tissues from MoM implants (Figure 4f).

The analysis mapped the side chain posttranslational modifications of several proteins (Supplement Table 1). Oxidations included the glutamic semi- aldehyde conversions of arginine, lysine, histidine, and tryptophan (Arg- >GluSA, Lys->Allysine, His->2-oxo-histidine, and Trp->Kynurenine) (Supplement Table 1). Analysis of the oxidatively damaged proteome indicated that proteins, related to different cellular function and sub-cellular location were oxidatively damaged (Figure 4g, Supplement Table 1). A directly proportional relationship between Cr levels and carbonyl content was observed in the periprosthetic tissues surrounding hip implants (Figure 4h).

Proteins in the MoM revision tissue proteome demonstrate binding affinity for Co and Cr. Immobilized-metal affinity chromatography (IMAC) was performed to separate metal- binding proteins from the total proteome extracted from periprosthetic tissues from

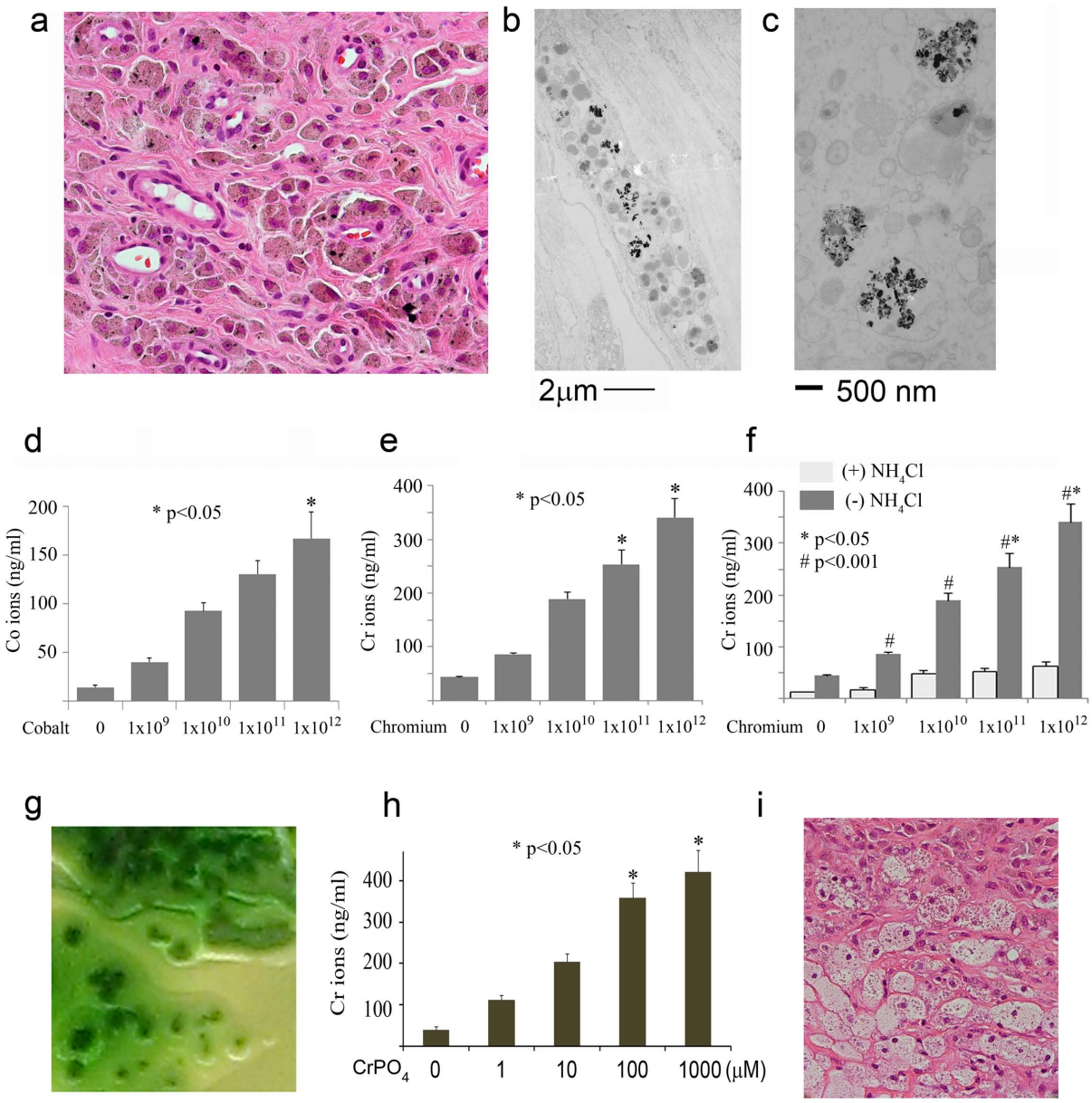

Figure 3 | Phagocytosis of Co or Cr nanoparticles by macrophages produces metal ions. (a) Light micrograph of a macrophagic infiltrate containing pale green corrosion product particles and black metallic particles in the periprosthetic tissue surrounding a resurfacing MoM implant, H-E staining. (b) Ultrastructural analysis of nanometer size metal wear debris/corrosion products phagocytosed by a macrophage present in periprosthetic tissue. (c) Transmission electron micrograph of metal wear nanoparticles accumulation in late endosomal compartments. (d) Bar graph and SDs of the spectrophotometric determination of Co ions release by primary macrophages cultured with Co nanoparticles. One way ANOVA ($p < 0.05$) was used to determine significance in treatment groups versus controls. (e) Bar graph and SDs of spectrophotometric determination of Cr ions release by primary macrophages cultured with Cr nanoparticles. One way ANOVA ($p < 0.05$) was used to determine significance in treatment groups versus controls. (f) Bar graph and SDs of spectrophotometric determination of Cr ions release by primary macrophages cultured with Cr nanoparticles in presence or absence of the lysosomal inhibitor ammonium chloride. One way ANOVA ($p < 0.05$) was used to determine significance in treatment groups versus controls. Tukey post hoc analysis ($p < 0.001$) was used to determine significant differences in treatment groups when compared to their respective treatment groups pre-treated with lysosomal inhibitors. (g) Light micrograph of prepared chromium orthophosphate ($CrPO_4$). (h) Bar graph and SDs of the spectrophotometric determination of Cr ions release by primary macrophages cultured with $CrPO_4$. One way ANOVA ($p < 0.05$) was used to determine significance in treatment groups versus controls. (i) Light micrograph of macrophages undergoing foamy degeneration in the periprosthetic tissue filled with corrosion product particles (H-E stain).

MoM implants. Metal-binding proteins were fractionated on the basis of their differential binding affinities of the surface exposed amino acids towards an immobilized metal ion. To determine if some of the known proteins with high affinity for metals could be retained by the IMAC columns charged with cobalt [Co(II)] and with chromium [Cr(III)], metal depleted tissue homogenates were loaded on an IMAC column/chip saturated with Co(II) or Cr(III). Proteins with affinity for binding Co(II) or Cr(III) were eluted from the immobilized columns with increasing concentrations of imidazole (Figures 5a, 5b). Recovered fractions were pooled into six groups and separated by 1D SDS-PAGE. Silver stain analysis of the SDS-PAGE indicated that several proteins present in the revision tissues surrounding MoM implants were able to bind Co(II) or Cr(III) (Figure 5c, Supplement Table 2). Following *in situ* tryptic

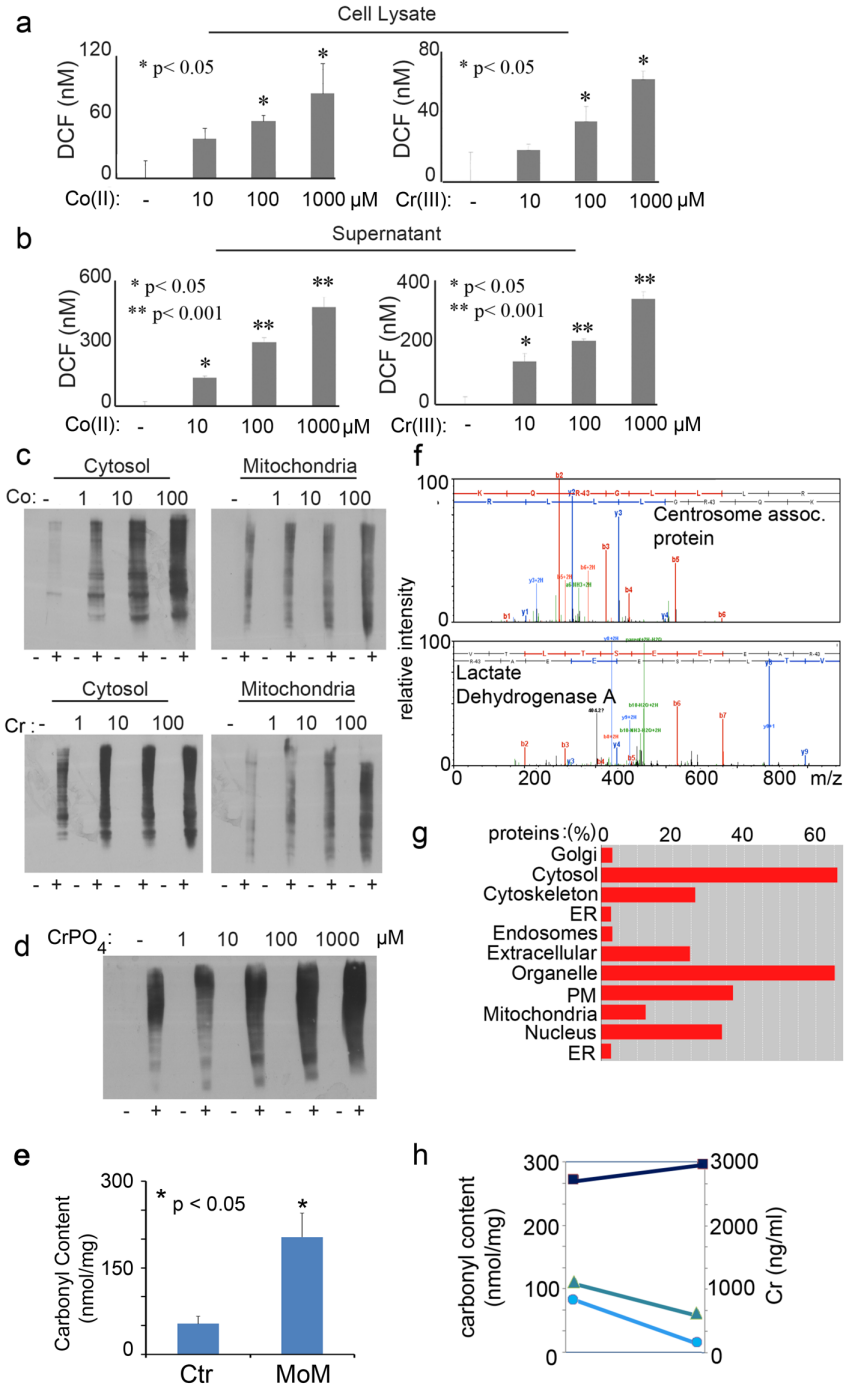

Figure 4 | Detection of oxidatively modified proteins following metal ion exposure. (a) Fluorometric measurement of reactive oxygen species (ROS) detected in lysates from primary macrophages, untreated or exposed to Co or Cr ions. One-way ANOVA, followed by the Tukey test ($p < 0.05$) was used to determine significant differences among and between groups. (b) Fluorometric measurement of reactive oxygen species (ROS) detected in the supernatants of primary macrophages, untreated or exposed to Co or Cr ions. One-way ANOVA, followed by the Tukey test ($p < 0.05$) was used to determine significant differences among and between groups. (c) Western blot analysis of oxidatively damaged carbonylated proteins detected in the cytosol and mitochondria isolated from of control and Co or Cr ions exposed primary macrophages. Lanes marked as "-" indicate non-derivatized proteins (derivatization control) and "+" indicate derivatized proteins. (d) Western blot analysis of carbonylated proteins detected in control and $CrPO_4$ treated primary macrophages. Lanes marked as "-" indicate non-derivatized proteins (derivatization control) and "+" indicate derivatized proteins. (e) Spectrophotometric quantification of oxidatively modified carbonylated proteins present in periprosthetic tissues surrounding control (CTR) and metal-on-metal (MoM) implants. Carbonyl content expressed as nmol carbonyl/mg protein One-way ANOVA, followed by the Tukey test ($p < 0.05$) was used to determine significant differences among and between groups. (f) MS/MS spectra of selected carbonylated proteins retrieved in the periprosthetic tissues surrounding MoM implants. The oxidized amino acid side chains are shown in the inset peptide sequence with their corresponding change in the molecular mass (K-1 = Allysine from K; R-43 = GluSA from R). The full list of the analyzed redox proteome is reported in Supplement Table 1. (g) Subcellular distribution of the oxidatively damaged proteome retrieved in the periprosthetic tissues surrounding MoM implants. The list of proteins is reported in Supplement Table 1. (h) Line graph comparing carbonyl content (nmol/mg) vs Cr (ng/ml) levels in periprosthetic tissues surrounding implants.

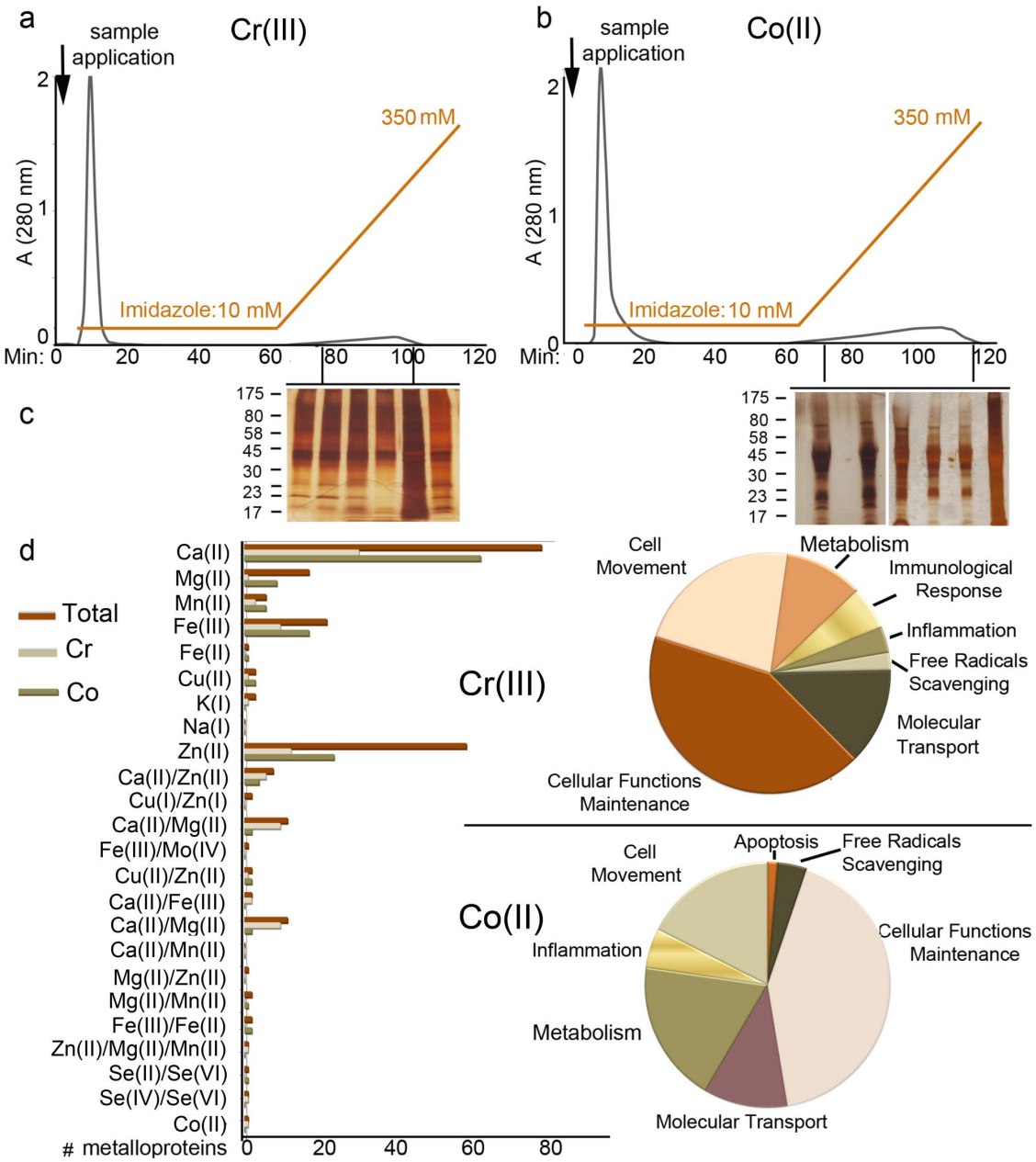

Figure 5 | Metal affinity chromatography with immobilized Cr(III) and Co(II)columns and bottom-up proteomics of the eluted metalloproteins. (a) Metal affinity chromatography on columns filled with Profinity IMAC resin immobilized with Cr(III)for the purification of metalloproteins with high affinity for Cr(III). 5 mg of protein from whole tissue homogenates extracted from the periprosthetic tissues surrounding MoM implants were loaded on the column and the metalloproteins eluted with increasing concentrations of imidazole (10–350 mM) after washing the unbound material with 10 mM imidazole. (b) Metal affinity chromatography on columns filled with Profinity IMAC resin immobilized with Co(II) for the purification of metalloproteins with high affinity for Co(II). 5 mg of proteins from whole tissue homogenates extracted from the periprosthetic tissues surrounding MoM implants were loaded on the column and the metalloproteins eluted with increasing concentrations of imidazole (10–350 mM) after washing the unbound material with 10 mM imidazole. (c) Silver staining of the SDS-PAGE gel (4–20%) used to separate six pooled fractions eluted with 10–350 mM imidazole gradient from the IMACs columns with Cr(III) and Co(II). Ten gel bands were cut across each sample lane and subjected to bottom-up proteomics analysis. (d) Proteins with different metals binding affinities bound to the IMACs columns with Cr(III) and Co(II) are shown as % from the total metalloproteins found in the total sample homogenate applied on each column. Bottom-up proteomics was performed using standard methods and the metal-bound proteins (presented in the Supplement Table 2) were assigned using Protein Knowledgebase (uniProtKB) (http://www.uniprot.org/) and MetalMine (http://metalmine.naist.jp/) databases.

digestion, extracted peptides were analyzed by nano LC–ESI–MS/MS on Orbitrap to identify the metal binding proteins in the revision tissues. Among the proteins eluted from the Cr(III)-loaded column were several enzymes such as enolase (Mg^{2+}), catalase (Fe(II)), myeloperoxidase (Fe(III)/Ca^{2+}), and arginase (Mn(II)), as well as molecular transporters such as ferritin (Fe(III)), hemoglobin (Fe(III)), ceruloplasmin (Cu(II)) and different Ca^{2+} binding proteins involved in many cellular functions (Figure 5d, Supplement Table 2). Similarly, among the protein eluted from the Co(II) column, there were several subunits of cytochrome C (Cu(II), Fe(III), and Zn(II) dependent), enzymes that are part of the cellular redox system, and Ca^{2+}-binding proteins important for cell motility and cell signaling (Figure 5d, Supplement Table 2). Altogether, pathway analysis of the cellular proteome binding Co(II) and Cr(III) columns indicate that

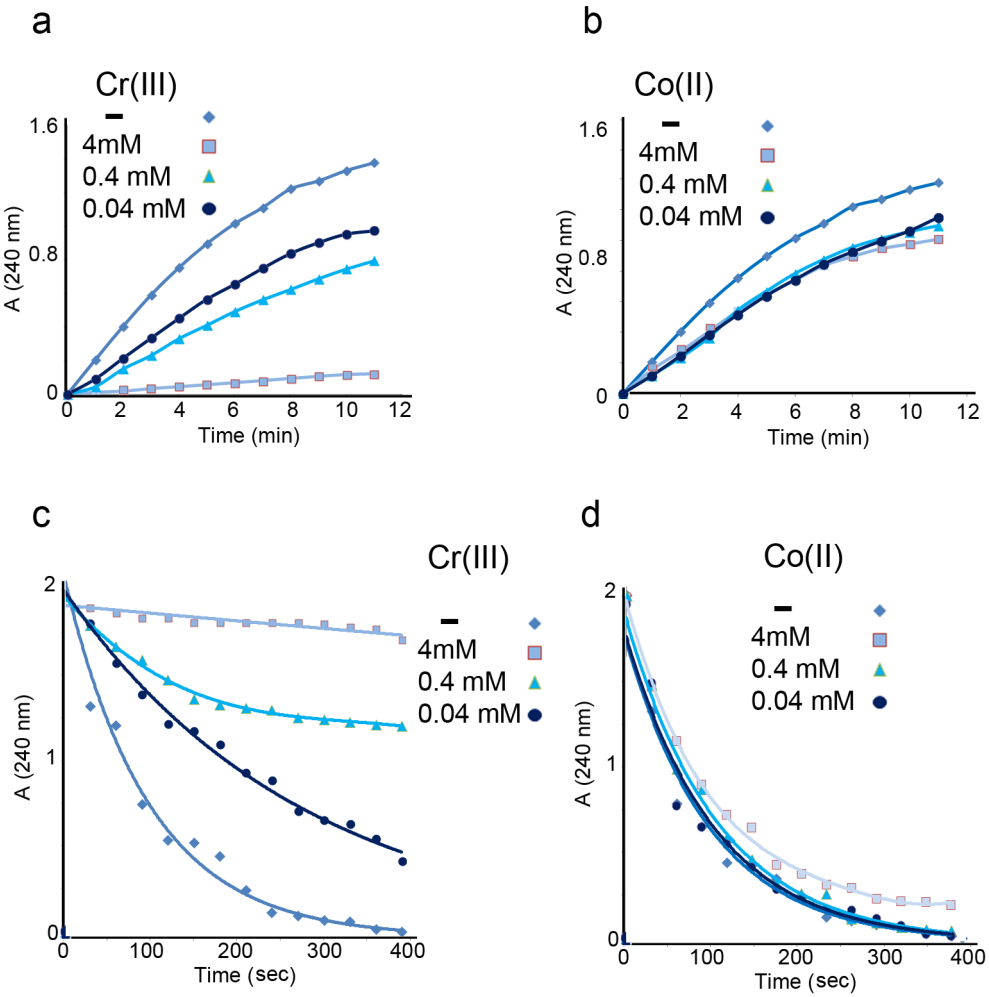

Figure 6 | Effects of Cr(III) and Co(II) on the *in vitro* aldolase and catalase activity. (a) Spectrophotometric analysis of hydrazone formation at 240 nm as a measurement of aldolase activity, in the absence or presence of Cr(III) (4 mM, 0.4 mM and 0.04 mM). (b) Spectrophotometric analysis of hydrazone formation at 240 nm as a measurement of aldolase activity, in the absence or presence of Co(II) (4 mM, 0.4 mM and 0.04 mM). c) Spectrophotometric analysis of H_2O_2 decomposition at 240 nm as an indication of catalase activity, in the absence or in the presence of Cr(III) (4 mM, 0.4 mM and 0.04 mM). (d) Spectrophotometric analysis of H_2O_2 decomposition at 240 nm as an indication of catalase activity, in the absence or in the presence of Co(II) (4 mM, 0.4 mM and 0.04 mM).

several cellular pathways and function could be potentially compromised by metal binding.

Chromium inhibits the catalytic activity of aldolase and catalase *in vitro*. To determine the potential effects of Co(II) or Cr(III) on cellular functions, we selected two enzymes; one, aldolase, which was previously reported to bind Cr(III) at a non-catalytic site[33]; and the other catalase, which could replace Fe(III) at its catalytic site with Cr(III). Fructose-bisphosphate aldolase (ALD), catalyzes a key reaction in glycolysis and energy production, i.e. the conversion of D-fructose-1,6-biphosphate into dihydroxyacetone phosphate and D-glyceraldehyde-3-phosphate. Thus, any impairment in this protein's catalytic activity would be followed by damage to the energetic balance of any cell[34]. The catalytic activity of pure human recombinant aldolase A was assessed to determine any enzymatic differences in the absence or presence of Co(II) or Cr(III) at different concentrations (4 mM, 0.4 mM and 0.04 mM for each Co(II) and Cr(III) solution). In each condition, the enzyme was incubated with the substrate, D-fructose 1,6-biphosphate, and hydrazine sulfate. The resulting hydrazone product, which absorbs at 240 nm, was measured. Spectrophotometric analysis of hydrazone formation demonstrated a dose dependent Cr(III) inhibition of aldolase activity, with complete loss of catalytic activity observed at 4 mM Cr(III) (Figure 6a). Interestingly, spectrophotometric measurements of hydrazone formation in the presence of Co(II) revealed minimal inhibition of aldolase activity at all concentrations used as compared with untreated aldolase (Figure 6b).

The second protein examined, catalase, is an enzyme responsible for the conversion of hydrogen peroxide to water and oxygen. Catalase is a tetramer consisting of four identical, tetrahedrally arranged subunits. Each 60 kDa subunit contains a heme group and NADPH in its active center[35]. Inhibitors of catalase include metals, which can affect heme structure via the displacement of iron. To examine the effects of metals on catalase function and possible alterations to catalytic activity, H_2O_2 decomposition was measured spectrophotometrically at 240 nm in the absence or presence of Co(II) or Cr(III). The presence of Cr(III) exerted a dose dependent inhibitory effect on catalase activity, with near abolishment of activity observed at 4 mM Cr(III) (Figure 6c) Spectrophotometric measurements of H_2O_2 decomposition in the presence of Co(II) at all concentrations, however, did not reveal any inhibition of catalase activity as compared to untreated catalase (Figure 6d). Together, these results indicate that Cr(III), but not Co(II), affects protein function in a dose dependent manner.

A comparison of Co(II) and Cr(III) toxicity from the *in vitro* and *ex vivo* results in this study is presented in Supplement Table 3. The most notable differences between the metal ions are: a linear correlation between Cr(III) concentration and protein carbonylation and a Cr(III) dose dependent inhibition of enzymatic catalytic activity (*in vitro*).

Discussion

Chromium and cobalt are minerals, both required as dietary supplements in trace amounts. The adequate daily intake for Cr is 25 to 50 μg/day and 5 to 8 μg/day for Co[36]. Both metals display toxic effects when present at high concentrations. Severe and irreversible cardiomyopathy and vision or hearing impairments are reported at serum Co concentrations over 700 μg/L, and reversible hypothyroidism and polycythemia at ~300 μg/L and higher[37–40]. For Cr acute oral toxicity ranges between 1900 and 3300 μg/kg and is associated with damage to multiple tissues and often kidney and liver failure[41]. Overexposure to both metals is sporadic and associated with environmental and/or industrial exposure. Recently, groups of patients implanted with hip devices of MoM bearing surface have been shown to develop an accelerated inflammatory reaction frequently associated with tissue necrosis and cellular toxicity. The sense of urgency in determining the molecular association between MoM implants and toxic response relates to the fact that there is a large population worldwide carrying these devices to be monitored long-term.

Metal-based implants release micrometer and nanometer sized wear debris, due to the tribocorrosion of the bearing surfaces[42]. The particulate metals released from the wear of joint implants are mostly colloidal CrCo alloys and likely some oxides (Cr_2O_3 and CoO). Herein we determined by TEM and light microscopy of periprosthetic tissues that these metal particles are readily phagocytosed by tissue resident macrophages and transported in endosomal and lysosomal compartments as indicated by the several observed phagocytic cells engulfed with corrosion product particles. In endosomal compartments, due to the presence of an acidic pH, the transition metals release Cr and Co ions with different oxidation states[43–46]. Induction of endosomal alkalinization greatly decreased metal ionization, with a direct correlation between the amount of phagocytosed metal particles, acid pH and released metal ions observed. This determination is important since metal ions are the ones associated with biological damage.

Indeed, increased amount of both Cr(III) and Co(II) were found in tissues retrieved from patients with MoM implants as compared with control implants including MoP, CoP, and CoC bearing surfaces which also may contain Cr and Co in their formulation but in much lower amounts. Cr(III) is the most thermodynamically stable species and does not tend to reduce to Cr(II) or oxidize to Cr(VI), which are more unstable oxidation states. Cr(VI), if present could be readily reduced to Cr(III)[47]. Cr(III) is the form mostly observed in patients with MoM "metallosis"[22,48,49] and it often forms complexes with the ubiquitously found, negatively charged phosphate group. The resulting Cr orthophosphate ($CrPO_4$) is commonly found in the periprosthetic tissue and the synovial fluid of patients with metal-on-metal-related pathology[43]. These precipitates are referred to as implant corrosion products. We observed these corrosion products both by TEM, where they present a globular and irregularly shaped appearance, and by histological analysis, as pale green intracellular and extracellular tissue deposits. The equilibrium kinetic between Cr(III) and its combined form ($CrPO_4$) and the conditions that skew the reaction toward free Cr(III) ion or its combined form will be worth exploring since these corrosion products serve as a constant source of metal ions that, since they cannot be disposed of, can amplify the tissue damage. Co(II) is the Co form mostly observed in patients with MoM "metallosis".

Our analysis on the effects of Cr and Co ions retrieved from MoM patients, indicate that several mechanisms account for the induced damage. First, Cr(III) and Co(II) catalyze the conversion of hydrogen peroxide (H_2O_2) into reactive hydroxyl radicals (HO•) in a chemical reaction known as the Fenton reaction[5]. Fenton chemistry is regularly known to occur in vivo; however, the level of activity is generally negligible due to only trace amounts of transition metals present in the human body. Additionally, under physiological conditions the cells are equipped with a variety of enzymes, including several isoforms of catalase, glutathione peroxidase and heme oxygenase-1, that dispose of ROS. When higher amounts of metal ions are present, however, the hydroxyl radicals formed by the metal-catalyzed Fenton reaction are greatly increased to levels that cannot be readily inactivated[50]. Excess ROS cause deleterious biological effects and irreversible damage by promoting protein, lipid, carbohydrate and DNA oxidation[50]. Importantly, we found a strong positive correlation between the amount of Cr and Co ions and tissue oxidative damage. Patients with the highest amount of Cr and Co ions present the highest levels of protein carbonylation, a well-known consequence of oxidative stress[50]. It is known that extensive oxidative modifications result in cleavage, sub-unit dissociation, unfolding, and aggregation, with an overall loss of biological function[51]. These conditions are effects of oxidative stress and are known to be associated with tissue degeneration and necrotic damage. High levels of oxidative stress can explain the necrotic tissue and formation of masses known as pseudotumors, observed in patients with MoM implants[17,18,27,52–55]. Our *in vivo* proteomic analyses indicate that several proteins associated with different cellular pathways are oxidatively damaged by Cr and Co-induced ROS. Having an overall carbonylated proteome could generally compromise cellular functions. Indeed, our *in vivo* data are further supported by several *in vitro* experiments indicating that Cr(III) induces cellular damage by activating ASK1 kinase, p38, Jun kinase and caspase 3[56]. Cobalt has also been shown to induce necrotic and apoptotic cell death[57].

As a second mechanism, Cr and Co metal ions can directly bind to proteins and directly induce oxidation and loss of biological function. It has been previously reported that Cr interacts with different serum proteins including hemoglobin, transferrin, and albumin[58]. Co has been proposed to bind to several proteins involved in the cellular redox system and ROS clearance[59].

Additionally, some of the toxic effects of Co(II) have recently been proposed to be due to inhibition of Ca^{2+} entry and Ca^{2+} signaling and competition with Ca^{2+} for intracellular Ca^{2+}- binding proteins[60]. Co(II) has also been shown to interact with various receptors, ion channels and biomolecules[13,61].

Our comprehensive proteomic analysis indicates that both Cr(III) and Co(II) can bind several more cellular proteins including enzymes involved in the cellular redox system (catalase, superoxide dismutase, glutathione peroxidase, metabolism (arginase 1, transglutaminase 3, enolase 1, molecular transport (transferritin, transcobalamin, hemoglobin, cellular motility (annexin A1, annexin A2, lymphocyte cytosolic protein 1, cell signaling (leukotriene A4 hydrolase, ryanodine receptor 2, phosphodiesterase 3A, cGMP-inhibited), and organelles functions. Altogether our data indicate that several cellular pathways and function can be potentially compromised by metal binding. As a proof of principle we determined that incubation of aldolase with Cr(III), and less so with Co(II), decreased the enzyme's ability to catalyze the formation of glyceraldehyde 3-phosphate from fructose 1–6 biphosphate, even though Cr(III) does not directly bind to the enzyme's catalytic site[33].

Finally, as a third mechanism, Cr and Co ions could displace other metal ions present in tissue metalloproteins and affect their activity. Indeed, protein elution from Cr(III) and Co(II) columns retrieved several metalloproteins among which Ca^{2+}, Fe(III) and Zn(II) binding proteins were particularly enriched. To determine whether Cr and Co ions can directly replace other ions present in metalloproteins we incubated catalase with Cr(III) ions since catalase contains a heme/Fe group in its active center[35]. A significant decrease in the catalytic ability of catalase to decompose H_2O_2 was observed.

In conclusion, our analyses indicate several mechanisms that can substantially explain the exaggerated tissue damage and accumulation of a large amount of necrotic macrophages in the joint fluid. Additional mechanisms, which were not mechanistically explored here, include the adverse tissue reactions associated with Cr and Co hypersensitivity, which are strongly dependent on the particle immunogenicity and patient immunological phenotype and can exponentially increase the inflammatory response.

Experimental procedure. *Mice and bone marrow macrophage (BMM) preparation*. C57BL/6 mice (3 months old) were purchased from Harlan Laboratories. Animal euthanasia and tissue harvesting were conducted according to a protocol approved by the Institutional Animal Care and Use Committee at Albert Einstein College of Medicine. Bone marrow cells were isolated from murine femurs and differentiated in M-CSF (10 ng/ml, RD Systems) for 5 days.

Primary macrophage cultures with metal nanoparticles and ions. In studies examining protein carbonylation and total free radical activity, cells were either left untreated or exposed to cobalt or chromium ions: cobalt (II) sulfate heptahydrate and chromium (III) chloride hexahydrate were prepared at concentrations of 1 μM, 10 μM, 100 μM in culture medium. For the spectroscopic analysis of metal ions, primary macrophages were incubated in the absence or presence of cobalt nanoparticles (purity 99.8%, a mean size of 28 nm) or chromium nanoparticles (purity 99.5%, a mean size of 50 nm, Nanostructured & Amorphous Materials, Inc., Houston, TX) or chromium orthophosphate (chromium (III) salt(1 : 1); phosphoric acid. Cobalt and chromium nanoparticles were suspended in culture medium at concentrations of 1×10^{10}, 10^{11}, 10^{12} particles per ml. In some experiments, prior to the addition of chromium nanoparticles, macrophages were pre-treated with a final concentration of 20 mM NH_4Cl and 0.1 mM Leupeptin to inhibit endosome-lysosome system acidification. In all experiments, control and exposed cells were collected 12 hours following treatment.

Histological analysis of revision tissues. Periprosthetic tissues were collected at surgery from a total of 9 cases undergoing revision surgery for adverse local tissue reactions (ALTR). All patients provided informed, written consent regarding participation in this study. Studies and procedures were conducted according to a protocol approved by the Albert Einstein College of Medicine Institutional Review Board. The implant group composition was as follows: MoM CoCr bearing surface, 9 [5 THA large head (>36 mm diameter) with metallic CoCr Mo sleeve adapter and 4 resurfacing implants with the same bearing surface]; Control (CTR) group was comprised of 9 samples: Metal-on-Polyethylene (MoP) bearing surface, 5; Ceramic-on-Polyethylene (CoP) bearing surface, 3; and Ceramic-on-Ceramic (CoC) bearing surface, 1; all with a conventional stem and monoblock modular neck. The tissue was collected fresh from several areas around the implant on ice. Collected tissues were fixed in 10% neutral buffered formalin and processed for hematoxylin-eosin staining. Sections were examined with a Zeiss Axioskop 40 microscope and images captured digitally using a ProgRes® camera (Jenoptik, Germany).

Backscatter scanning electron microscopy and Energy-dispersive X-ray spectroscopic (EDS) analysis of wear debris powder. Wear debris powder was gently scraped or shaken from the implant metallic sleeves with a sterile carbon steel metallic surgical blade and saved in an OPTICLEAR® 15 × 45 mm screw thread borosilicate glass vial w rubber lined cap (Kimble Chase, Rockwood, TN) prior to analysis. Using carbon paste as an adhesive, powders were sprinkled onto a carbon stub and then coated with carbon. Spectra and maps were collected on a Zeiss Supra 40 FESEM with Oxford INCA energy dispersive spectrometer at 10 kV.

ICP-MS sample preparation and instrumental conditions. Each sample was mixed with 0.5 mL of *aqua regia*, and then the sample was diluted to 10 ml with de-ionized water. A series of standard solutions of Co and Cr were prepared under the same acidic conditions. The inductively-coupled plasma (ICP) mass spectrometry (MS) measurements were performed on a PerkinElmer NexION 300X ICP mass spectrometer. ^{59}Co and ^{52}Cr were measured under the kinetic energy discrimination (KED) mode.

Spectrophotometric determination of protein carbonyl content. The carbonyl content of revision tissues and primary macrophages exposed to metal ions was quantified spectrophotometrically with the Protein Carbonyl Assay kit (Cayman Chemical Company, Ann Arbor, MI).

Western blot analysis of carbonyl groups. Revision tissue homogenates and primary cell lysates were prepared in 150 mM NaCl, 50 mM Tris, 1 mM EDTA, and 1% NP40. Prepared samples were derivatized using the Oxyblot Protein Oxidation Detection Kit (Millipore, USA), separated on 4–15% SDS-PAGE, and transferred membranes were incubated with a rabbit polyclonal anti-DNP antibody followed by a goat anti-rabbit IgG–HRP antibody. Proteins were visualized by chemiluminescence.

Transmission electron microscopy. Periprosthetic tissues, collected fresh on ice, were immediately fixed in 2.5% glutaraldehyde, 2% paraformaldehyde, in sodium cacodylate buffer 0.1 M, pH 7.4 for 3 hours at 4°C, post-fixed in 1.0% aqueous osmium tetroxide, and embedded in LX112-Araldite (Ted Pella Inc, CA, USA). Ultrathin sections were stained with uranyl acetate followed by lead citrate, and viewed with a Jeol JEM-1200EX transmission electron microscope (Jeol Ltd., Akishima, Japan) at 80 kV.

Fluorometric measurement of total ROS activity. The total free radical activity in control and metal ion exposed primary macrophages and culture supernatants was quantified with the OxiSelect *In Vitro* ROS/RNS Assay kit (Cell Biolabs, Inc., San Diego, CA).

Spectroscopic determination of cobalt (II) ions. Cobalt (II) concentrations in total cell lysates prepared from control and cobalt nanoparticle (Co^0) exposed primary macrophages were measured following the incubation with a solution containing 0.8 ml 6 M HCl, 2.0 ml 50% potassium thiocyanate in 4.8 ml acetone. The absorbance of the complexes of cobalt ions with thiocyanate was measured spectrophotometrically at 620 nm.

Colorimetric determination of chromium (VI) ions. Chromium (VI) concentrations in control and chromium nanoparticle (Cr^0) exposed primary macrophages and culture supernatants were determined following the incubation with a solution containing 0.5 ml 3 M H_2SO_4, 0.5 ml 50% 1.5-Diphenylcarbazide in 9.0 ml deionized water. The absorbance was measured spectrophotometrically at 540 nm.

Organelle isolation and cytosol preparation. Cytosol was prepared was isolated from homogenates following centrifugation for 1 h at 100,000 g at 4°C. Mitochondria were isolated from homogenates following two consecutive centrifugations for 10 minutes each at 7,000 g at 4°C.

FPLC gel filtration fractionation of the proteome contained in the homogenates from revision tissues. Extracted proteins (about 5–6 mg of each homogenate from at least five patient revision tissues) were run through a Superdex S200 gel filtration column (HiLoad 16/60) coupled to a Bio-Rad FPLC system interfaced with Biologic DuoFlow software. One representative run consisted of 240 ml of PBS buffer with 300 mM NaCl, pH 7.4, run through the column at a flow rate of 0.5 ml/min.

rLys-C/trypsin digestion of the proteome. Multiple fractions were lyophilized before mass spectroscopy analysis and subjected to reduction and alkylation. Fractions were digested first with endoproteinase Lys-C followed by trypsin.

NanoLC-ESI-MS/MS analysis of Lys-C/tryptic peptides. Lys-C/tryptic digests were analyzed by nano LC/MS/MS with a Waters NanoAcquity HPLC system interfaced to a ThermoFisher Q Exactive with the Orbitrap operating at 60,000 FWHM and 17,500 FWHM for MS and MS/MS respectively. The fifteen most abundant ions were selected for MS/MS.

Database searching. Raw tandem mass spectra data files were extracted, converted to mgf files using Proteome Discoverer version 1.3, and analyzed using Mascot (Matrix Science, London, UK). Mascot was set up to search the SwissProt-2013-07 database (selected for Homo sapiens, 20265 entries) Mascot was searched with a fragment ion mass tolerance of 0.80 Da and a parent ion tolerance of 10.0 PPM. For the redox proteome analysis we used as variable modifications the amino acids oxidations reported in Mascot.

Validation of the posttranslational (PTM) modifications and normalizing spectral counts. The proteins were considered identified having at least one bold red (BR) significant peptide with an ion score cut-off of 20 or greater (corresponding to $p < 0.05$ and a FDR proteins <1.0). Scaffold (Proteome Software Inc., Portland, OR) was used to validate MS/MS based peptide and protein identifications.

Immobilized metal affinity chromatography (IMAC) purification of metalloproteins. IMAC columns were charged with either Co(II) or Cr(III) (300 mM in PBS, pH 6.5). Columns were equilibrated in 50 mM NaH_2PO_4 with 10 mM imidazole and 0.3 M NaCl at 1 ml/min flow rate using the Bio-Rad FPLC system interfaced with Biologic DuoFlow software. 5 mg of protein homogenates were loaded on each IMAC column and 1 ml fractions were collected for the entire run. Eluted fractions at 20–350 mM imidazole were further fractionated on 1D 4%–20% SDS-PAGE and subsequently silver stained. 10 gel bands were cut across each sample lane and subjected to bottom-up proteomics analysis. *In situ* endoproteinase Lys-C and tryptic digestion was performed after reduction and alkylation. Extracted tryptic peptides were analyzed by nano LC–ESI–MS/MS on Orbitrap and the data were processed with Proteome Discoverer, Mascot and Scaffold.

Aldolase catalytic activity. Using the Boyer modification of the hydrazine assay[62], in which 3-phosphoglyceraldehyde reacts with hydrazine to form a hydrazone product which absorbs at 240 nm, we designed a microassay in which pure human recombinant aldolase A (1–364 aa) (50 μg/assay mixture) was left untreated or incubated with different concentrations of the two heavy metals (4 mM, 0.4 mM and 0.04 mM for each Co(II) and Cr(III) solution) in the presence of the substrate, D-fructose 1,6-biphosphate (4.0 mM final concentration) and hydrazine sulfate (about 2.5 mM final concentration) in PBS at pH 7.4. The formation of the hydrazone was characterized by an increase in the absorption at 240 nm monitored over 10–15 min incubation time.

Catalase catalytic activity. To test the inhibition of catalase by Co(II) and Cr(III) we developed a microassay adapted from the Worthington's assay[63] in which the disappearance of peroxide is followed spectrophotometrically at 240 nm. 20–50 μg of pure protein (from human erythrocytes) were incubated in an assay mixture containing 0.05 M potassium phosphate, pH 7.0 and 0.059 M hydrogen peroxide (30%) in 0.05 M potassium phosphate, pH 7.0 as the substrate. The consumption of peroxide was monitored in the presence or absence of Co(II) or Cr(III) using the same concentration range as in the aldolase assay.

1. Anderson, R. A. Chromium as an essential nutrient for humans. *Regul Toxicol Pharmacol* **26**, S35–41, doi:10.1006/rtph.1997.1136 (1997).
2. Mertz, W. Chromium occurrence and function in biological systems. *Physiol Rev* **49**, 163–239 (1969).
3. Hodgkin, D. C. *et al*. Structure of vitamin B12. *Nature* **178**, 64–66 (1956).
4. Klaassen, C. D., Casarett, L. J. & Doull, J. *Casarett and Doull's toxicology: the basic science of poisons*. 8th edn, (McGraw-Hill, 2013).
5. Beyersmann, D. & Hartwig, A. Carcinogenic metal compounds: recent insight into molecular and cellular mechanisms. *Arch Toxicol* **82**, 493–512, doi:10.1007/s00204-008-0313-y (2008).
6. ASTDR. (ed Public Health Service U.S. Department of Health and Human Services) 1–592 (2012).
7. Barceloux, D. G. Chromium. *J Toxicol Clin Toxicol* **37**, 173–194 (1999).
8. Keegan, G. M., Learmonth, I. D. & Case, C. P. A systematic comparison of the actual, potential, and theoretical health effects of cobalt and chromium exposures from industry and surgical implants. *Crit Rev Toxicol* **38**, 645–674, doi:10.1080/10408440701845534 (2008).
9. ATSDR. 1–417 (U.S. Department of Health and Human Services, Public Health Service, 2004).
10. Barceloux, D. G. Cobalt. *J Toxicol Clin Toxicol* **37**, 201–206 (1999).
11. McDermott, P. H., Delaney, R. L., Egan, J. D. & Sullivan, J. F. Myocardosis and cardiac failure in men. *JAMA* **198**, 253–256 (1966).
12. Morin, Y. & Daniel, P. Quebec beer-drinkers' cardiomyopathy: etiological considerations. *Can Med Assoc J* **97**, 926–928 (1967).
13. Paustenbach, D. J., Tvermoes, B. E., Unice, K. M., Finley, B. L. & Kerger, B. D. A review of the health hazards posed by cobalt. *Crit Rev Toxicol* **43**, 316–362, doi:10.3109/10408444.2013.779633 (2013).
14. Bozic, K. J. *et al*. The epidemiology of bearing surface usage in total hip arthroplasty in the United States. *J Bone Joint Surg Am* **91**, 1614–1620, doi:10.2106/JBJS.H.01220 (2009).
15. Huber, M., Reinisch, G., Trettenhahn, G., Zweymuller, K. & Lintner, F. Presence of corrosion products and hypersensitivity-associated reactions in periprosthetic tissue after aseptic loosening of total hip replacements with metal bearing surfaces. *Acta Biomater* **5**, 172–180, doi:10.1016/j.actbio.2008.07.032 (2009).
16. Higgs, G. B. *et al*. Is Increased Modularity Associated With Increased Fretting and Corrosion Damage in Metal-On-Metal Total Hip Arthroplasty Devices?: A Retrieval Study. *J arthroplasty* **28**, 2–6 (2013).
17. Xia, Z. *et al*. Characterization of metal-wear nanoparticles in pseudotumor following metal-on-metal hip resurfacing. *Nanomedicine* **7**, 674–681, doi:10.1016/j.nano.2011.08.002 (2011).
18. Sampson, B. & Hart, A. Clinical usefulness of blood metal measurements to assess the failure of metal-on-metal hip implants. *Ann Clin Biochem* **49**, 118–131, doi:10.1258/acb.2011.011141 (2012).
19. Hart, A. J. *et al*. The chemical form of metallic debris in tissues surrounding metal-on-metal hips with unexplained failure. *Acta Biomater* **6**, 4439–4446, doi:10.1016/j.actbio.2010.06.006 (2010).
20. Merritt, K. & Brown, S. A. Release of hexavalent chromium from corrosion of stainless steel and cobalt-chromium alloys. *J Biomed Mater Res* **29**, 627–633, doi:10.1002/jbm.820290510 (1995).
21. Shettlemore, M. G. & Bundy, K. J. Examination of in vivo influences on bioluminescent microbial assessment of corrosion product toxicity. *Biomaterials* **22**, 2215–2228 (2001).
22. De Smet, K. *et al*. Metal ion measurement as a diagnostic tool to identify problems with metal-on-metal hip resurfacing. *J Bone Joint Surg Am* **90 Suppl 4**, 202–208, doi:10.2106/JBJS.H.00672 (2008).
23. Hart, A. J. *et al*. Sensitivity and specificity of blood cobalt and chromium metal ions for predicting failure of metal-on-metal hip replacement. *J Bone Joint Surg Br* **93**, 1308–1313, doi:10.1302/0301-620X.93B10.26249 (2011).
24. Daniel, J., Ziaee, H., Pradhan, C. & McMinn, D. J. Six-year results of a prospective study of metal ion levels in young patients with metal-on-metal hip resurfacings. *J Bone Joint Surg Br* **91**, 176–179, doi:10.1302/0301-620X.91B2.21654 (2009).
25. Dunstan, E. *et al*. Metal ion levels after metal-on-metal proximal femoral replacements: a 30-year follow-up. *J Bone Joint Surg Br* **87**, 628–631, doi:10.1302/0301-620X.87B5.15384 (2005).
26. Schaffer, A. W., Pilger, A., Engelhardt, C., Zweymueller, K. & Ruediger, H. W. Increased blood cobalt and chromium after total hip replacement. *J Toxicol Clin Toxicol* **37**, 839–844 (1999).
27. Pandit, H. *et al*. Pseudotumours associated with metal-on-metal hip resurfacings. *J Bone Joint Surg Br* **90**, 847–851, doi:10.1302/0301-620X.90B7.20213 (2008).
28. Willert, H. G. *et al*. Metal-on-metal bearings and hypersensitivity in patients with artificial hip joints. A clinical and histomorphological study. *J Bone Joint Surg Am* **87**, 28–36, doi:10.2106/JBJS.A.02039pp (2005).
29. Catelas, I. & Wimmer, M. A. New insights into wear and biological effects of metal-on-metal bearings. *J Bone Joint Surg Am* **93 Suppl 2**, 76–83, doi:10.2106/JBJS.J.01877 (2011).
30. Auffan, M., Rose, J., Wiesner, M. R. & Bottero, J. Y. Chemical stability of metallic nanoparticles: a parameter controlling their potential cellular toxicity in vitro. *Environ Pollut* **157**, 1127–1133, doi:10.1016/j.envpol.2008.10.002 (2009).
31. Kwon, Y. M. *et al*. Dose-dependent cytotoxicity of clinically relevant cobalt nanoparticles and ions on macrophages in vitro. *Biomed Mater* **4**, 025018, doi:10.1088/1748-6041/4/2/025018 (2009).

32. Petit, A. *et al.* Induction of protein oxidation by cobalt and chromium ions in human U937 macrophages. *Biomaterials* **26**, 4416–4422, doi:10.1016/j.biomaterials.2004.11.019 (2005).
33. Ertunga, N. S. *et al.* Cloning, expression, purification and characterization of fructose-1,6-bisphosphate aldolase from Anoxybacillus gonensis G2. *J Biochem* **141**, 817–825, doi:10.1093/jb/mvm085 (2007).
34. Macomber, L., Elsey, S. P. & Hausinger, R. P. Fructose-1,6-bisphosphate aldolase (class II) is the primary site of nickel toxicity in Escherichia coli. *Mol Microbiol* **82**, 1291–1300, doi:10.1111/j.1365-2958.2011.07891.x (2011).
35. Scibior, D. & Czeczot, H. [Catalase: structure, properties, functions]. *Postepy Hig Med Dosw (Online)* **60**, 170–180 (2006).
36. Trumbo, P., Yates, A. A., Schlicker, S. & Poos, M. Dietary reference intakes: Vitamin A, vitamin K, arsenic, boron, chromium, copper, iodine, iron, manganese, molybdenum, nickel, silicon, vanadium, and zinc. *J Am Dietetic Assoc* **101**, 294–301, doi:Doi 10.1016/S0002-8223(01)00078-5 (2001).
37. Bowie, E. A. & Hurley, P. J. Cobalt chloride in the treatment of refractory anaemia in patients undergoing long-term haemodialysis. *Aust N Z J Med* **5**, 306–314 (1975).
38. Davis, J. E. & Fields, J. P. Experimental production of polycythemia in humans by administration of cobalt chloride. *Proc Soc Exp Biol Med* **99**, 493–495 (1958).
39. Finley, B. L., Monnot, A. D., Paustenbach, D. J. & Gaffney, S. H. Derivation of a chronic oral reference dose for cobalt. *Regul Toxicol Pharmacol* **64**, 491–503, doi:DOI 10.1016/j.yrtph.2012.08.022 (2012).
40. Jaimet, C. H. & Thode, H. G. Thyroid function studies on children receiving cobalt therapy. *J Am Med Assoc* **158**, 1353–1355 (1955).
41. Katz, S. A. & Salem, H. The Toxicology of Chromium with Respect to Its Chemical Speciation - a Review. *J Appl Toxicol* **13**, 217–224, doi:DOI 10.1002/jat.2550130314 (1993).
42. Bowsher, J. G., Hussain, A., Williams, P. A. & Shelton, J. C. Metal-on-metal hip simulator study of increased wear particle surface area due to 'severe' patient activity. *Proc Inst Mech Eng H* **220**, 279–287 (2006).
43. Davda, K., Lali, F. V., Sampson, B., Skinner, J. A. & Hart, A. J. An analysis of metal ion levels in the joint fluid of symptomatic patients with metal-on-metal hip replacements. *J Bone Joint Surg Br* **93**, 738–745, doi:10.1302/0301-620X.93B6.25804 (2011).
44. Dobbs, H. S. & Minski, M. J. Metal ion release after total hip replacement. *Biomaterials* **1**, 193–198 (1980).
45. Luetzner, J., Krummenauer, F., Lengel, A. M., Ziegler, J. & Witzleb, W. C. Serum metal ion exposure after total knee arthroplasty. *Clin Orthop Relat Res* **461**, 136–142, doi:10.1097/BLO.0b013e31806450ef (2007).
46. McPhee, I. B. & Swanson, C. E. Metal ion levels in patients with stainless steel spinal instrumentation. *Spine (Phila Pa 1976)* **32**, 1963–1968, doi:10.1097/BRS.0b013e318133aa0d (2007).
47. Newton, A. W., Ranganath, L., Armstrong, C., Peter, V. & Roberts, N. B. Differential distribution of cobalt, chromium, and nickel between whole blood, plasma and urine in patients after metal-on-metal (MoM) hip arthroplasty. *J Orthop Res* **30**, 1640–1646, doi:10.1002/jor.22107 (2012).
48. Jacobs, J. J. *et al.* Local and distant products from modularity. *Clin Orthop Relat Res,* 94–105 (1995).
49. Kadoya, Y. *et al.* Wear particulate species and bone loss in failed total joint arthroplasties. *Clin Orthop Relat Res,* 118–129 (1997).
50. Cannizzo, E. S., Clement, C. C., Sahu, R., Follo, C. & Santambrogio, L. Oxidative stress, inflamm-aging and immunosenescence. *J Proteomics* **74**, 2313–2323, doi:10.1016/j.jprot.2011.06.005 (2011).
51. Scharf, B. *et al.* Age-related carbonylation of fibrocartilage structural proteins drives tissue degenerative modification. *Chem Biol* **20**, 922–934, doi:10.1016/j.chembiol.2013.06.006 (2013).
52. Billi, F. & Campbell, P. Nanotoxicology of metal wear particles in total joint arthroplasty: a review of current concepts. *J Appl Biomater Biomech* **8**, 1–6 (2010).
53. Campbell, P. *et al.* Histological features of pseudotumor-like tissues from metal-on-metal hips. *Clin Orthop Relat Res* **468**, 2321–2327, doi:10.1007/s11999-010-1372-y (2010).
54. Grammatopoulos, G. *et al.* The correlation of wear with histological features after failed hip resurfacing arthroplasty. *J Bone Joint Surg Am* **95**, e81, doi:10.2106/JBJS.L.00775 (2013).
55. Pandit, H. *et al.* Necrotic granulomatous pseudotumours in bilateral resurfacing hip arthoplasties: evidence for a type IV immune response. *Virchows Arch* **453**, 529–534, doi:10.1007/s00428-008-0659-9 (2008).
56. Rudolf, E. & Cervinka, M. Trivalent chromium activates Rac-1 and Src and induces switch in the cell death mode in human dermal fibroblasts. *Toxicol Lett* **188**, 236–242, doi:10.1016/j.toxlet.2009.04.019 (2009).
57. Rovetta, F. *et al.* Cobalt triggers necrotic cell death and atrophy in skeletal C2C12 myotubes. *Toxicol Appl Pharmacol* **271**, 196–205, doi:10.1016/j.taap.2013.05.005 (2013).
58. Tkaczyk, C. *et al.* Investigation of the binding of Cr(III) complexes to bovine and human serum proteins: a proteomic approach. *J Biomed Mater Res A* **94**, 214–222, doi:10.1002/jbm.a.32700 (2010).
59. Ray, P. D., Huang, B. W. & Tsuji, Y. Reactive oxygen species (ROS) homeostasis and redox regulation in cellular signaling. *Cell Signal* **24**, 981–990, doi:10.1016/j.cellsig.2012.01.008 (2012).
60. Simonsen, L. O., Harbak, H. & Bennekou, P. Cobalt metabolism and toxicology--a brief update. *Sci Total Environ* **432**, 210–215, doi:10.1016/j.scitotenv.2012.06.009 (2012).
61. Simonsen, L. O., Brown, A. M., Harbak, H., Kristensen, B. I. & Bennekou, P. Cobalt uptake and binding in human red blood cells. *Blood Cells Mol Dis* **46**, 266–276, doi:10.1016/j.bcmd.2011.02.009 (2011).
62. Jagannathan, V., Singh, K. & Damodaran, M. Carbohydrate metabolism in citric acid fermentation. 4. Purification and properties of aldolase from Aspergillus niger. *Biochem J* **63**, 94–105 (1956).
63. Beers, R. F., Jr. & Sizer, I. W. A spectrophotometric method for measuring the breakdown of hydrogen peroxide by catalase. *J Biol Chem* **195**, 133–140 (1952).

Acknowledgments

VZ is supported by the PhD program in Genetics and cell Biology at the University of Tuscia, Department of Ecology and Biology(DEB), Viterbo, Italy.

Author contributions

B.S., G.P., E.P., S.G., N.C., R.V., L.S. wrote the main manuscript text. B.S., C.C., G.P., L.S. prepared figures 1–6. B.S., C.C., V.Z., G.P., B.Y., G.E., F.M. performed the experiments. All authors reviewed the manuscript.

Additional information

Supplementary information accompanies this paper at http://www.nature.com/scientificreports

Competing financial interests: The authors declare no competing financial interests.

How to cite this article: Scharf, B. *et al.* Molecular analysis of chromium and cobalt-related toxicity. *Sci. Rep.* **4**, 5729; DOI:10.1038/srep05729 (2014).